We now consider a numerical test of the model in the case of a two-dimensional mixing layer in the configuration shown in Fig. 2. Propane is injected through a narrow slot into a stream of air. In the first step, no combustion is taken into account. Only contact area is considered and the nonpremixed reactants mix to form a premixed stream. When the flow is well established, ignition takes place from the initial premixed flame area distributed at time $t = O$ around the ignition point.

The contours of constant mass fractions of nonpremixed fuel, premixed fuel, densities of contact, premixed and diffusion flame areas and temperature are displayed in Fig. 3 as a function of time. Combustion begins with an unsteady premixed flame propagating in the initial mixture. The flame front travels crosswise and then propagates upstream inside the recirculation zone. A diffusion flame is then ignited and reaches a stationary configuration while the premixed flame disappears with the consumption of all the premixed reactants. This description is in qualitative agreement with a high-speed schlieren film of the ignition phase of an experimental combustor with the same geometrical configuration. The steady-state structure of the established diffusion flame is also in agreement with previous numerical simulations and experiments (Lacas et al.[7]).

## IV. Conclusions

A model is proposed for turbulent flames combining premixed and nonpremixed flamelets. This model is tested in a simple case to simulate the transient post ignition regime of a diffusion flame. Further computations are being conducted to qualify the combined model. It will be useful to compare numerical predictions with experimental results, but the available data are not adequate. However, preliminary calculations indicate that it may be possible to describe time-evolving-situations or the steady-state stabilization of nonpremixed shear flows. Further tests should prove whether this model is able to simulate blow-off and lift-off of diffusion flames. The formulation may be improved in various ways. For example, it will be easy to add other terms in the balance equations for the different flame surface densities to predict the quenching phenomenon due to excessively large local strain rates.

## References

[1]Marble, F. E., and Broadwell, J. E., "The Coherent Flame Model for Turbulent Chemical Reactions," TRW, EL Segundo, CA Project Squid Rept. TRW-9-PU, 1977.

[2]Peters, N., "Laminar Diffusion Flamelets in Nonpremixed Turbulent Combustion," *Progress in Energy and Combustion Science*, Vol. 10, No. 3, 1984 p. 319.

[3]Peters, N., "Laminar Flamelets Concepts in Turbulent Combustion," 21st *Symposium (International) on Combustion,* Combustion Inst., Pittsburgh, PA, 1986.

[4]Bray, K. N. C., "Methods of Including Realistic Chemical Mechanisms in Turbulent Combustion Models," *Second Workshop on Modeling of Chemical Reaction Systems,* Heidelberg, Germany, 1986.

[5]Veynante, D., Lacas, F., and Candel, S. M., "A New Flamelet Combustion Model Combining Premixed and Nonpremixed Turbulent Flames," AIAA Paper 89-0487, Jan. 1989.

[6]Veynante, D., Candel, S. M., and Martin, J. P., "Coherent Flame Modeling of Chemical Reactions in a Turbulent Mixing Layer," *2nd Workshop on Modeling of Chemical Reaction Systems*, Heidelberg, Germany, 1986.

[7]Lacas, F., Zikikout, S., and Candel, S. M., "A Comparison Between Calculated and Experimental Mean Source Terms in Nonpremixed Turbulent Combustion," AIAA Paper 87-1782, 1987.

[8]Darabiha, N., Giovangigli, V., Trouve, A., Candel, S. M. and Esposito, E., "Coherent Flame Description of TurbuLent Premixed Ducted Flames," *Workshop on Turbulent Combustion,* Rouen, France, 1987.

[9]Dupoirieux, F., and Scherrer, D., "Méthodes Numeriques à Convergence Rapide Utilisées pour le Calcul des Ecoulements Réactifs," *1st Symposium on Numerical Simulation of Combustion Phenomena,* Sophia-Antipolis, France, May 1985.

# Numerical Solutions of the Incompressible Navier-Stokes Equations with Boundary Condition Switching

Z. Fang*and I. Paraschivoiu†
*École Polytechnique de Montréal, Montréal, Québec, H3C 3A7 Canada*

## Introduction

THE boundary condition switching method for solving stream function-vorticity equations[1,2] is applied to solve the incompressible Navier-Stokes equations in primitive variable form. The key idea of this method is that on boundaries, where both Dirichlet and Neumann boundary conditions are known, the Neumann boundary condition is satisfied naturally while the Dirichlet boundary condition is used to substitute the unknown boundary condition of the other variable, for instance, vorticity in stream function-vorticity equations and pressure in Navier-Stokes equations. When solving the Navier-Stokes equations with primitive variables for incompressible laminar flows, the Dirichlet boundary condition is the velocity boundary condition by giving zero velocity at wall boundaries. The Neumann boundary condition are given by the continuity condition. In the methods solving Navier-Stokes equations with primitive variables, the velocity boundary conditions are implemented with the Neumann boundary condition satisfied by continuity equation. It is well known that these methods result in pressure oscillations using equal-order interpolation in finite element method[3] (FEM) and using non-staggered grid in finite difference method[4] (FDM). This difficulty could be removed by using the present method. Application of the present method is tested by both FEM and FDM. Our results show that this method does not result in any pressure oscillations. Thus, pressure solutions do not need to be filtered or smoothed.

## Governing Equations and Boundary Conditions

The two-dimensional steady incompressible Navier-Stokes equations are

$$V \cdot \nabla V + \nabla P/\rho = \nu \nabla^2 V \tag{1}$$

$$\nabla \cdot V = 0 \tag{2}$$

in a bounded domain $\Omega$, where $V$ is the velocity vector, $P$ the pressure, $\rho$ the density, and $\nu$ the kinematic viscosity. Boundary conditions are

$$V = V(x) \qquad \text{on } \Gamma_1 \in \Gamma \equiv \partial\Omega \tag{3}$$

$$\frac{\partial V}{\partial n} = \frac{\partial V}{\partial n}(x) \qquad \text{on } \Gamma_2 \in \Gamma \equiv \partial\Omega \tag{4}$$

$$P = P(x) \qquad \text{on } \Gamma_3 \in \Gamma \equiv \partial\Omega \tag{5}$$

where $\Gamma_1 \cup \Gamma_2 \cup \Gamma_3 = \Gamma$.

On some boundaries both Dirichlet and Neumann boundary conditions for velocity exist when a viscous flow problem is

Received Dec. 21, 1989; revision received May 8, 1990; accepted for publication May 20, 1990. 

*Research Associate, Department of Mechanical Engineering, P. O. Box 6079, Station A. Member AIAA.

†J.-A. Bombardier Aeronautical Chair Professor, Department of Mechanical Engineering, P. O. Box 6079, Station A. Member AIAA.

solved. To implement boundary conditions in a numerical procedure, sometimes Neumann boundary conditions are ignored. For example, along a horizontal solid wall, the no-penetration condition is implemented explicitly by giving $v = 0$. The Neumann boundary condition along walls $\partial v/\partial y = 0$ is satisfied automatically by the continuity equation. In the present procedure, the condition $\partial v/\partial y = 0$ is implemented explicitly in both FEM and FDM while the no-penetration condition $v = 0$ is used to replace the continuity equation for the pressure representation. On other wall boundaries, boundary conditions can be implemented similarly.

## Finite Element Formulation

The weighted residual formulation is applied and the integration weak forms of Eqs. (1) and (2) are

$$\iint_\Omega W(V \cdot \nabla V + \nabla P/\rho - \nu \nabla^2 V)\, d\sigma = 0 \tag{6}$$

$$\iint_\Omega W(\nabla \cdot V)\, d\sigma = 0 \tag{7}$$

where $W$ is the weighting function. In Eq. (6), applying Green transformation to the second-order term and choosing the weighting function $W$ to be the shape function $N$, we have

$$\iint_\Omega [N(V \cdot \nabla V + \nabla P/\rho) + \nu \nabla N \cdot \nabla V]\, d\sigma = \int_\Gamma \nu N \frac{\partial V}{\partial n}\, dS \tag{8}$$

The derivative of the normal component of velocity at the walls is zero and satisfied automatically because the boundary integral for the velocity normal component in Eq. (8) vanishes. Thus, the no-penetration condition can be used to replace the continuity equation for pressure representation.

Bilinear elements are used in this work and the appropriate piecewise polynomial basis functions for velocity $V$ and pressure $P$ are

$$V = \sum_{k=1}^{4} N_k V_k \tag{9}$$

$$P = \sum_{k=1}^{4} N_k P_k \tag{10}$$

The discretized simultaneous equations are built up using the local stiffness matrix:

$$A = \begin{bmatrix} K_{u,u} & 0 & K_{u,p} \\ 0 & K_{v,v} & K_{v,p} \\ K_{p,u} & K_{p,v} & 0 \end{bmatrix} \tag{11}$$

where

$$K_{u,u} = \iint (NV \cdot \nabla u + \nu \nabla N \cdot \nabla u)\, d\sigma$$

$$K_{u,p} = \iint N \frac{\partial P}{\partial x} \frac{1}{\rho}\, d\sigma$$

$$K_{v,v} = \iint (NV \cdot \nabla v + \nu \nabla N \cdot \nabla v)\, d\sigma$$

$$K_{v,p} = \iint N \frac{\partial P}{\partial y} \frac{1}{\rho}\, d\sigma$$

$$K_{p,u} = \iint N \frac{\partial u}{\partial x}\, d\sigma, \qquad K_{p,v} = \iint N \frac{\partial v}{\partial y}\, d\sigma$$

and $u$ and $v$ are the $x$ and $y$ components of the velocity $V$.

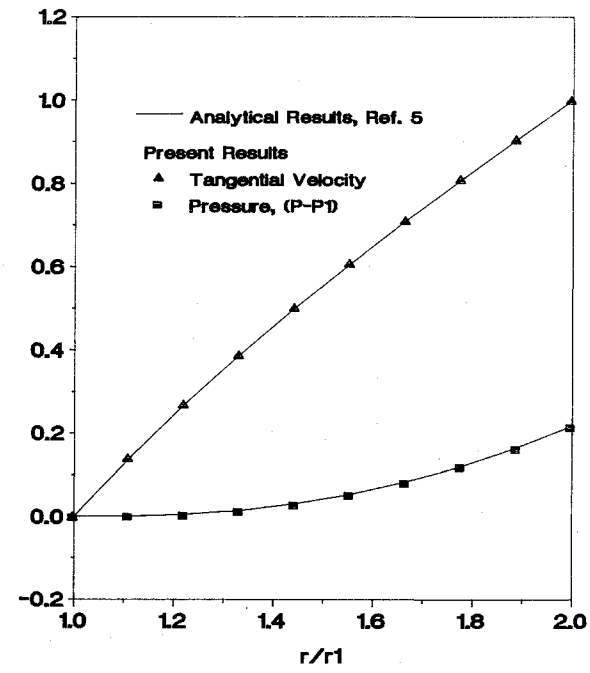


Fig. 1 Results on rotating cylinders.

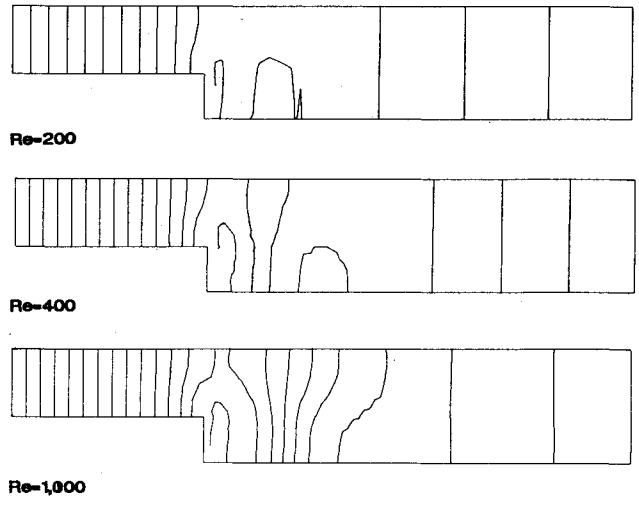


Fig. 2 Pressure contours in the duct.

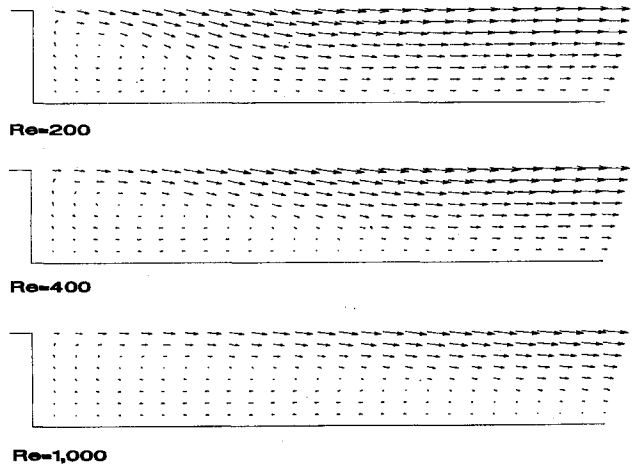


Fig. 3 Velocity field in the duct.

### Finite Difference Formulation

The central difference formulation is used for grid points inside the domain. Thus, the finite difference equations for grid point $(i,j)$ are

$$u_{i,j}^{n-1}\frac{\bar{\delta}_x u_{i,j}^n}{2\Delta x}+v_{i,j}^{n-1}\frac{\bar{\delta}_y u_{i,j}^n}{2\Delta y}+\frac{\bar{\delta}_x P_{i,j}^n}{2\Delta x}-Re^{-1}\left[\frac{\bar{\delta}_x^2 u_{i,j}^n}{\Delta x^2}+\frac{\bar{\delta}_y^2 u_{i,j}^n}{\Delta y^2}\right]=0 \tag{12}$$

$$u_{i,j}^{n-1}\frac{\bar{\delta}_x v_{i,j}^n}{2\Delta x}+v_{i,j}^{n-1}\frac{\bar{\delta}_y v_{i,j}^n}{2\Delta y}+\frac{\bar{\delta}_y P_{i,j}^n}{2\Delta y}-Re^{-1}\left[\frac{\bar{\delta}_x^2 v_{i,j}^n}{\Delta x^2}+\frac{\bar{\delta}_y^2 v_{i,j}^n}{\Delta y^2}\right]=0 \tag{13}$$

$$\frac{\bar{\delta}_x u_{i,j}^n}{2\Delta x}+\frac{\bar{\delta}_y v_{i,j}^n}{2\Delta y}=0 \tag{14}$$

where

$$\bar{\delta}_x q_{i,j}=q_{1+1,j}-q_{1-1,j} \tag{15}$$

$$\bar{\delta}_y q_{i,j}=q_{1,j+1}-q_{1,j-1} \tag{16}$$

$$\delta_x^2 q_{i,j}=q_{1+1,j}-2q_{i,j}+q_{1-1,j} \tag{17}$$

$$\delta_y^2 q_{i,j}=q_{1,j+1}-2q_{i,j}+q_{1,j-1} \tag{18}$$

The Neumann boundary conditions for the normal component of velocity at the wall can be satisfied automatically if we apply the finite difference equations for the momentum equations to grid points on boundaries where both Dirichlet and Neumann boundary conditions exist. For instance, for horizontal wall boundaries, we have $u=0$, $v=0$, and $\partial v/\partial y=0$. Thus, Eq. (13) becomes

$$\frac{\Delta P_{i,j}^n}{\Delta y}+Re^{-1}\left[\frac{2\Delta v_{i,j}^n}{\Delta y^2}\right]=0 \tag{19}$$

The Dirichlet boundary condition $v=0$ is used to replace the continuity equation. In this way, both Dirichlet and Neumann boundary conditions are implemented with the continuity equation satisfied. For grid points inside the flow region, Eqs. (12–14) are implemented and for grid points on the wall boundaries, the momentum equations take the form of Eq. (19). These equations are solved simultaneously while the nonlinear system is updated by Newton-Raphson method. With the boundary condition switching, staggered grids are not necessary and there is no pressure oscillation found.

### Results and Discussions

The first test flow problem is the incompressible laminar flow between concentric rotating cylinders. The exact solution can be found in textbooks on fluid mechanics (see, e.g., Schlichting[5]). Numerical solutions for this problem can be compared with the exact solution to estimate the accuracy. In this test case, the inner cylinder with radius $r_1$ is stationary and the outer cylinder with radius $r_2$ rotates with angular velocity $\omega$. The dimensionless primitive variable form of the Navier-Stokes equations in polar coordinates is solved. Velocity components are nondimensionalized with respect to the outer cylinder tangential velocity $r_2\omega$. All lengths are nondimensionalized with respect to the inner radius $r_1$. The dimensionless pressure is defined by $P/\rho(r_2\omega)^2$ and the radius ratio $r_2/r_1$ is fixed at 2. In this problem, a $10\times 16$ mesh is employed. Both FEM and FDM are applied on the same grid. Numerical results obtained by both methods are very close to each other. Numerical results show that the dimensionless solutions of this problem are independent of Reynolds number. In Fig. 1, tangential velocity distribution is shown as a function of $r/r_1$. The relative pressure $P-P_i$ is also plotted in Fig. 1. Good agreement between our numerical results and the analytical solution can be seen.

The second flow problem solved with the present method is the flow in a duct with the sudden enlargement. The definition of the flowfield geometry is $1.5H$ at the duct inlet and $2.5H$ at the duct exit with a back-step heigh $H$. The length of the duct from the back step to duct exit is $20H$ and the length from duct inlet to the back step is $9H$. The computation was performed for Reynolds numbers of 200, 400, and 1000 on a grid with 2169 grid points. The present method is implemented on the same grid with both FEM and FDM. The dimensionless pressure $P/[(\rho_\infty V_\infty^2)/2]$ contours are shown in Fig. 2. Pressure values change continually and smoothly along the duct. There is no spurious pressure value observed. Thus, the pressure-filtering procedure is not needed. Velocity fields in the region close to the back step are shown in Fig. 3. At the duct inlet and the duct exit, velocity profiles present fully developed laminar flows. Near the back step a circulation zone is observed. For higher Reynolds number the reattachment point moves further downstream.

### Acknowledgment

This work was supported by the National Sciences and Engineering Research Council of Canada.

### References

[1]Peeters, M. F., Habashi, W. G., and Dueck, E. G., "Finite-Element Stream Function-Vorticity Solutions of the Incompressible Navier-Stokes Equations," *International Journal for Numerical Methods in Fluids,* Vol. 7, No. 4, 1987, pp. 17–27.

[2]Habashi, W., Peeters, M., Guevremont, G., and Hafes, M., "Finite-Element Solutions of the Compressible Navier-Stokes Equations," *AIAA Journal,* Vol. 25, No. 7, 1987, pp. 944–948.

[3]Sani, R. L., Gresho, P. M., Lee, R. L., and Griffiths, D. F., "The Cause and Cure (?) of the Spurious Pressure Generated by Certain FEM Solutions of the Incompressible Navier-Stokes Equations: Pt. 1," *International Journal for Numerical Methods in Fluids,* Vol. 1, No. 1, 1981, pp. 17–43.

[4]Strikwerda, J. C., "Finite-Difference Methods for the Stokes and Navier-Stokes Equations," *SIAM Journal on Scientific and Statistical Computing,* Vol. 5, No. 1, 1984, pp. 56–68.

[5]Schlichting, H., *Boundary-Layer Theory,* McGraw-Hill, New York, 1968, Chap. 5.

# Forebody Vortex Control with the Unsteady Bleed Technique

D. R. Williams* and H. Papazian†
*Illinois Institute of Technology, Chicago, Illinois 60616*

## I. Introduction

THE asymmetric system of vortices that separate from the forebodies of aircraft and missiles at high angles of attack has long been recognized as a significant contributor to the aerodynamic loading on the vehicle.[1–3] Strong yaw moments are created that can overwhelm the control surfaces causing the vehicle to lose control. For example, the unpredictable trajectories of missiles launched at high angles of attack are related to the forces generated by the forebody vortices.

Received March 19, 1990; revision received May 9, 1990; accepted for publication May 9, 1990. 

*Associate Professor, Fluid Dynamics Research Center. Member AIAA.

†Former Graduate Research Assistant, Fluid Dynamics Research Center.